From Superhydrophobic- to Superhydrophilic-Patterned Poly(vinylidene fluoride-co-chlorotrifluoroethylene) Architectures as a Novel Platform for Biotechnological Applications

Vanessa F. Cardoso, [1,2] Ana R. Machado, [1] Vânia C. Pinto, [2] Paulo J. Sousa, [2] Gabriela Botelho, [3] Graça Minas, [2] Senentxu Lanceros-Méndez [1,4,5]

[1] Centro/Departamento De Física, Universidade Do Minho, Campus De Gualtar, Braga 4710-057, Portugal

[2] CMEMS-UMinho, Universidade Do Minho, DEI, Campus De Azurém, Guimarães 4800-058, Portugal

[3] Centro/Departamento De Química, Universidade Do Minho, Campus De Gualtar, Braga 4710-057, Portugal

[4] Parque Científico Y Tecnológico De Bizkaia, BCMaterials, Derio 48160, Spain

[5] Basque Foundation for Science, IKERBASQUE, Bilbao, Spain

Correspondence to: V. F. Cardoso (E-mail: vanessa@dei.uminho.pt); S. Lanceros-Méndez (E-mail: lanceros@fisica.uminho.pt)

Abstract

The manufacture of three-dimensional patterned electroactive poly(vinylidene fluoride-co-chlorotrifluoroethylene) microstructures with tailored architecture, morphology, and wettability is presented. The patterned microstructures are fabricated using a simple, effective, low cost, and reproducible technique based on microfluidic technology. These novel structures can represent innovative platforms for advanced strategies in a wide range of biotechnological applications,

KEYWORDS: hydrophobicity; patterned microstructures; polydimethylsiloxane; poly(vinylidene fluoride-co-chlorotrifluoroethylene); SU-8

INTRODUCTION Membranes and structures with tailored porosity and morphology are being increasingly used in the biotechnology area for applications including scaffolds for cells growth and tissue engineering, [1] drug delivery systems, [2] energy harvesting, [3] wastewater treatment, [4] and sensors and actuators. [5] Among the different materials that can be used to produce such porous structures, polymers arise as the most promising due to the possibility of tailoring morphology, chemical, thermal and mechanical properties, as well as, biodegradability to meet specific requirements. In addition, the class of smart polymer materials can lead to the development of functional and responsive structures for use in shape memory, electroactive or magnetoactive devices, [6] among others. In the biomedical field and related areas, one of the most widely used is the electroactive piezoelectric response. [7]

Poly(vinylidene fluoride) (PVDF) and its copolymers present the largest piezoelectric response among the polymers. [8] PVDF is a high molecular weight semicrystalline polymer that can exhibit five distinct crystalline phases, being the α and β-phases the most desirable from a technological point of view. Nevertheless, the β-phase is the one that exhibits the highest piezoelectric, pyroelectric, and ferroelectric properties. Further, PVDF and its copolymers show an excellent combination of processability, biocompatibility, mechanical, chemical, and thermal resistances. [9] Copolymers, such as poly(vinylidene fluoride-co-hexafluoropropylene) (PVDFHFP), poly(vinylidenefluoride-co-trifluoroethylene (PVDFTrFE), and poly(vinylidene fluoride-co-chlorotrifluoroethylene) P(VDF-CTFE), have been developed to obtain specific tailored properties, which include polymer phase, morphology, crystallinity, melting temperature, ionic conductivity and mechanical properties, among others, to meet precise requirements of emerging applications in the areas of energy, [10] tissue engineering, [11] and filtration. [12] This is the case of P(VDF-CTFE) copolymer that has been applied as battery separators and filtration membranes. [13–15]

Different techniques have been used for the fabrication of PVDF-based membranes, including solvent casting, sintering, spin-coating, dip-coating, electrospinning, stretching and phase inversions, among others. [8] These techniques allow producing single or multilayer membranes with different

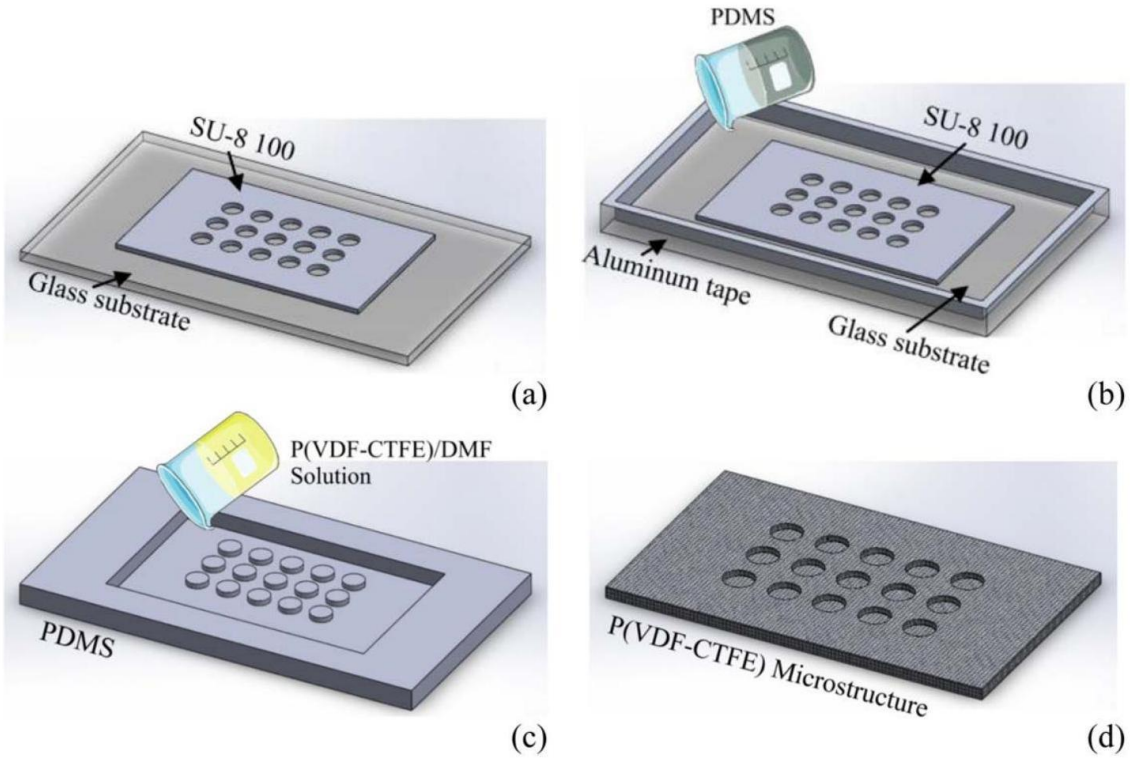

FIGURE 1 Schematic representation of the processing steps to obtain patterned P(VDF-CTFE) microstructures: (a) fabrication of the SU-8 mold on glass substrate; (b) placement of aluminum tape and deposition of the PDMS solution followed by curing at 80 °C on a hotplate for 2 h ; (c) deposition of the P(VDF-CTFE)/DMF solution on the PDMS mold previously discarded from the SU-8 mold, followed by a heat treatment at a specific temperature; (d) final patterned P(VDF-CTFE) microstructure. [Color figure can be degrees of porosity and pore size but they are limited in their ability to create patterned three-dimensional structures. [16]

This work reports on a simple, effective, low cost and reproducible technique based on microfluidic strategies to fabricate multifunctional three-dimensional patterned P(VDFCTFE) microstructures with tailored architecture, morphology, wettability and electroactive response. Six microstructures with two different configurations-arrays of pillars or wells-and three different dimensions-diameter/height (pillars) and diameter/depth (wells) of ~ 100,250, and 400 μm, separated by the same distance-were fabricated. A schematic representation of the various manufacturing steps for obtaining P(VDF-CTFE) microstructures is shown in Figure 1. The procedure involved the fabrication of two molds: the first mold in SU-8 photoresist was fabricated using a low cost photolithography process [Fig. 1(a)], which was used to fabricate the second-one, in polydimethylsiloxane (PDMS) by replica molding [Fig. 1(b)]. The final P(VDF-CTFE) microstructure was obtained using the PDMS mold and heat treatment at specific temperatures [Fig. 1(c,d)]. SU-8 and PDMS are two materials typically used in microfluidic technology for biotechnology and related applications, [17,18] which allow the development of structures in the micro- and nanoscale range with well-known and standardized processing procedures. [19,20] The SU-8 and PDMS structures have the advant-
age of allowing repeated use without damage, reducing the cost of manufacturing processes.

The unique characteristics of the developed novel polymerbased structures, including superhydrophobic and superhydrophilic behaviors, tailored architecture, and electroactive polymer phase, represent innovative platforms for advanced applications.

RESULTS AND DISCUSSION

Morphology Characterization

Three different drying temperatures were studied to fabricate P(VDF-CTFE) microstructures with different morphologies. Figure 2 shows representative surface and crosssectional SEM images of flat P(VDF-CTFE) membranes, that is, without pillars and wells.

It is shown that the membranes dried at 25 °C [Fig. 2(a)] are white and show a high degree of porosity, formed by large ($\sim 3.1 \pm 0.6\mu$ m diameter) and nanoporous (approximate pore dimension of 100 ± 24 nm) spherulites. Increasing drying temperature [Fig. 2(b,c)] leads to translucent membranes, as the porosity decreases and the membrane become thinner, due to a mostly compact cross section. However, the surface of the P(VDF-CTFE) membranes in contact with the PDMS molds shows some roughness due to the small porous

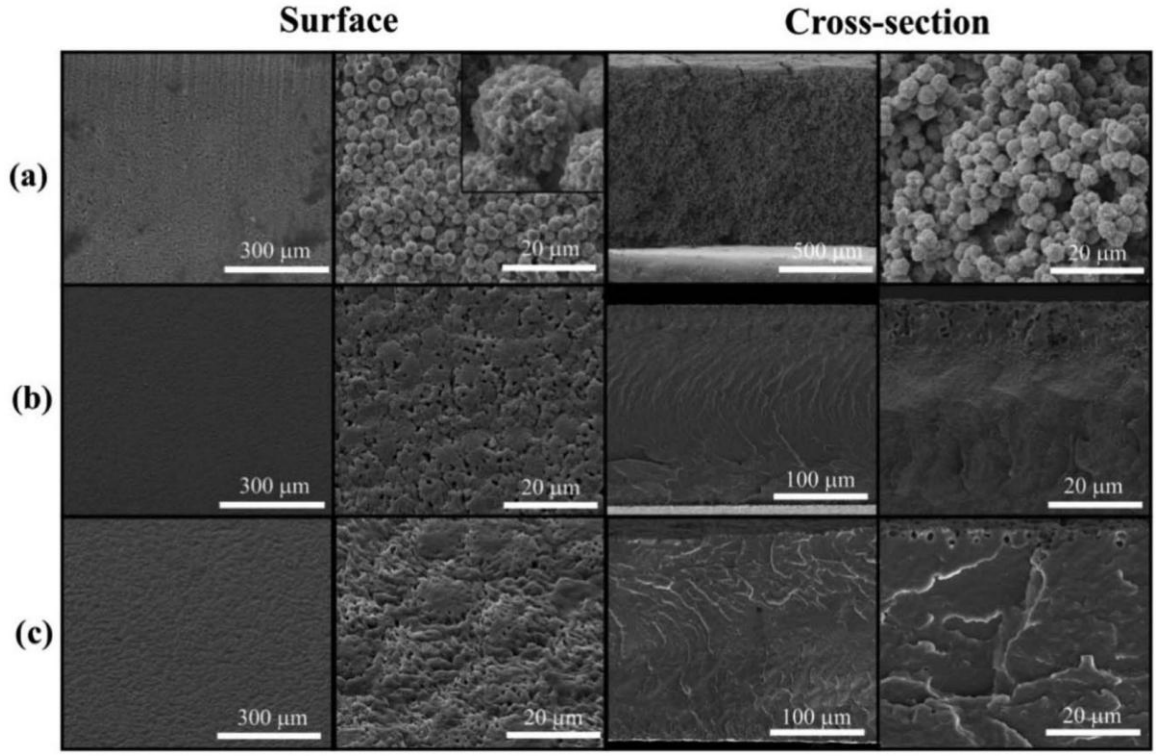

FIGURE 2 Representative SEM images of flat P(VDF-CTFE) membranes (without pillars or wells) obtained at different drying temperatures: (a) 25°C; (b) 50°C; (c) 75°C. layer on its surface, as can be seen in the cross-sectional view with higher amplification. This surface porous layer decreases with increasing drying temperature from 50 to 75 °C.

The evaporation rate of the solvent plays an important role on the morphology obtained and depends on various factors, including copolymer/solvent volume fraction of the solution, initial thickness of the membrane and drying temperature. Generally, the pore formation is described by the polymer-solvent diagram where higher drying temperatures lead to higher solvent evaporation rates, which in turn avoid the formation of pores. [14,21] In this specific case, a gradient of solvent evaporation rate across the cross section of the membrane is expected: close to the surface in contact with air (opposite to the PDMS mold) a high evaporation rate occurs, also promoted by the convective heat flow inside the oven, avoiding the formation of pores and leading to a crystallized P(VDF-CTFE) skin layer. This fact combined with the high initial thickness of the membrane lead to a slower evaporation rate near the PDMS mold and to the possible formation of pores, as occur in the membranes dried at 50 and 75 °C. It is expected that at higher drying temperatures, fully dense, and transparent P(VDF-CTFE) membranes can be obtained. [14] However, this can affect significantly the electroactive β-phase content of the samples (as it will be discussed further) and, consequently, their piezoelectric performance, inhibiting their use in applications as piezoelectric sensors and actuators. [7]

Figure 3 shows representative SEM images of patterned P(VDF-CTFE) microstructures fabricated at the drying temperatures of 25 and 75 °C. The indicated dimensions correspond to the predefined diameters and heights of the pillars and wells of the initial SU-8 molds.

It is observed that the dimensions of the P(VDF-CTFE) pillars and wells are smaller than the initial SU-8 molds, with a mean reduction of ~ 15%, which can be explained by the solvent evaporation and arrangement of the polymer chains during crystallization. All patterned P(VDF-CTFE) microstructures are well defined, being the surface morphologies very similar to the flat (PVDF-CTFE) membranes (Fig. 2) for the same drying temperature. Thus, the patterned P(VDFCTFE) microstructures dried at 25 °C present a complex porous morphology constitute by arrays of threedimensional pillars or wells composed by large and nanoporous spherulites. Consequently, three different dimensions are presented: the micrometer dimensions of the pillars/ wells arrays (dimensions referred previously), the micrometer dimensions of the spherulites ($\sim 3.1 \pm 0.6 \mu$m) and the nanometer dimensions of the spherulites pores ($\sim 100 \pm 24$ nm). At higher drying temperatures, that is, 50 and 75 °C, the surface morphology of the patterned P(VDF-CTFE) microstructures become smoother and the cross-sectional dense and compact as presented in Figure 2(b,c). These microstructural features will have a major effect on the

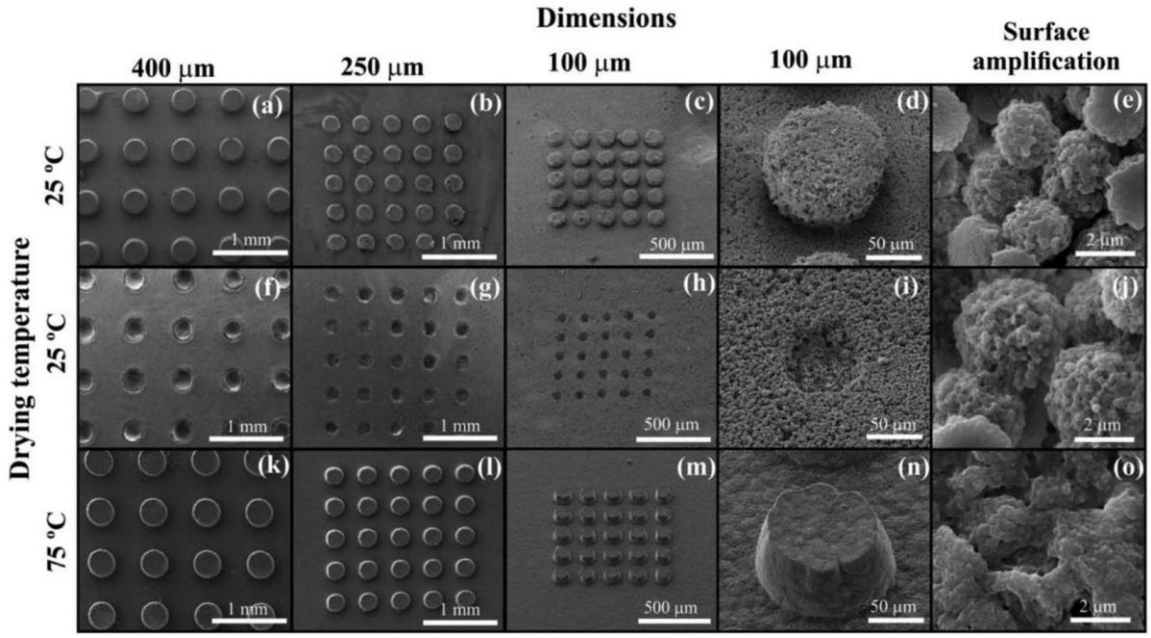

FIGURE 3 Representative SEM images of patterned P(VDF-CTFE) microstructures obtained at different drying temperatures. hydrophobicity of the patterned P(VDF-CTFE) microstructures (see below sections).

Others patterned microstructures can be obtained, which depend mainly on the limitation of the SU-8 molds fabricated. It is important to notice that the PDMS molds can be used numerous times, reducing the fabrication costs for multiple microstructures.

Water Surface Contact Angle Measurements

Surface characteristics, including membrane hydrophobicity, play an important role in technological application such as scaffolds for tissue engineering, [11] battery and fuel cell membranes, [22] lab-on-a-chip systems, [23] water purification membranes, [24] and biosurfaces, [25] among others. Contact angle measurement is a simple and effective method commonly used to evaluate the surface wettability of a membrane. It is influence by various factors such as the surface energy of the material, the surface roughness, and the surface tension of the liquid. [26] Static contact angles of the flat and patterned P(VDF-CTFE) microstructures are presented in Figure 4. The fitting mode used for the measurement of the contact angles is of major importance since for the same water droplet different contact angles can be obtained. [22] In this work, circle fitting was used. Generally, a surface is called hydrophilic when its contact angle is lower than 90°, whereas a hydrophobic surface shows a contact angle higher than 90°. A turning point of 65° between hydrophilic and hydrophobic is however also used. [27] Nonetheless, a surface can be called superhydrophobic when its contact angle is close to or higher than 150°, [27] and superhydrophilic for contact angles close or lower than 10°.[28]

A liquid water features a relatively high surface tension mainly due to is electrical dipole. [27] As a result, a water drop will tend to bead-up surfaces that present a low surface energy

and will tend to wet surfaces with high surface energy. Therefore, fluorinated polymers, as it is the case of P(VDF-CTFE), exhibit strong hydrophobicity due to their low surface energy. [29] This observation was confirmed by the measurement of the static contact angle of the flat P(VDFCTFE) membranes, presented in Figure 4, all of them showing a contact angle higher than 100°. Moreover, the contact angle increases with decreasing drying temperature. This result is verified in all P(VDF-CTFE) microstructures (flat and patterned) and it is explained by the increase of roughness of the surface associated to the increase of the surface

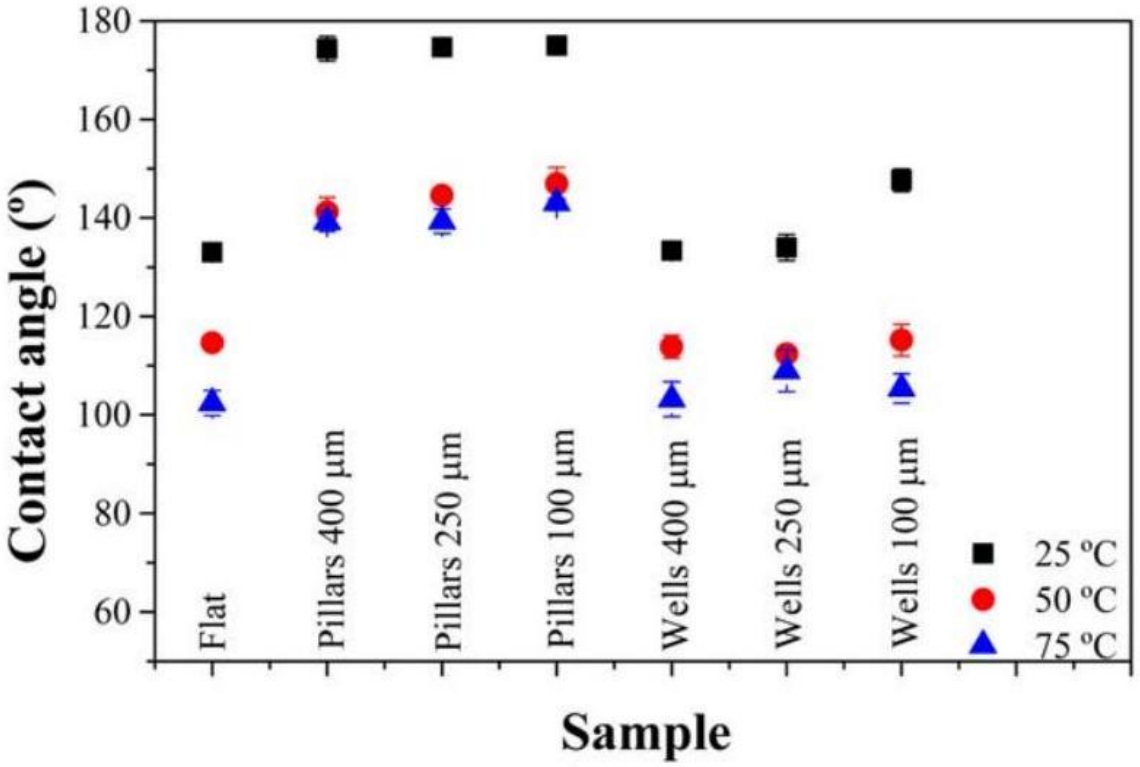

FIGURE 4 Static contact angles of the P(VDF-CTFE) samples. [Color figure can be viewed in the online issue, which is available at wileyonlinelibrary.com.]

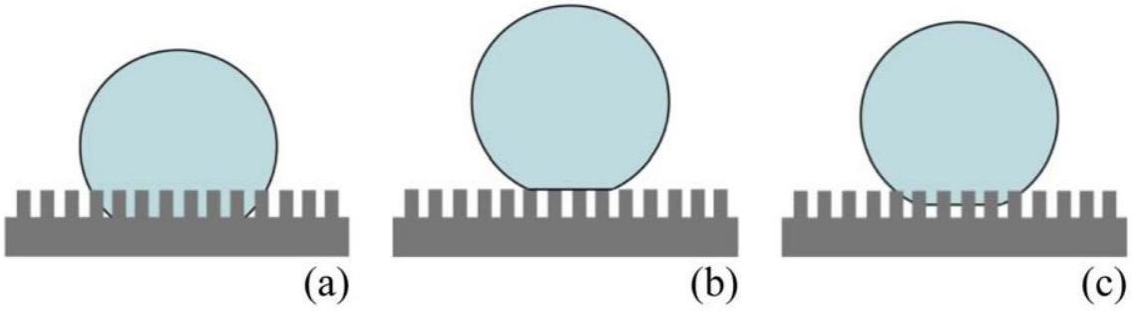

FIGURE 5 Wetting regimes: (a) Wenzel; (b) Cassie-Baxter; (c) combined Cassie-Baxter/Wenzel.

porosity with decreasing the drying temperature, as stated previously. The hydrophobicity of a material is generally enhanced by the presence of surface textures, which is attributed to the increase of the effective surface area. [30] This result, however, is only verified in initially slightly hydrophobic solid surface with contact angle higher than 90°.[31] In this present work, the addition of pillars to the P(VDF-CTFE) membranes dried at 25 °C increase the contact angle from 138° in flat membranes to higher than 174° in pillars-based microstructures. Therefore, the surfaces become superhydrophobic due to the complex and highly rough surface presented by the arrays of three-dimensional pillars composed by large and nanoporous spherulites. The measurement of the contact angle at the surface of the pillars was complicated by the fact that the water drop seems to be "repelled" by the surface and clung to the needle tip (Supporting Information, Video S1). Consequently, it is possible to expect that these microstructures follow the Cassie-Baxter regime [Fig. 5(b)] allowing the drops of water to roll off easily on their surfaces, similar to the "lotus effect," which is responsible for self-cleaning properties. [22] In contrast, increasing the drying temperature of the pillars-based P(VDF-CTFE) microstructures, the contact angles decrease and the surfaces seem to follow a combined Cassie-Baxter/Wenzel state [Fig. 5(c)], where the water drop stick to the pillars, even turning the sample 180° (Supporting Information Video S2). [23,32]

Regarding the wells-based microstructures, the measured contact angles are very close to the contact angles of the corresponding flat P (VDF-CTFE) membranes, which means that under these experimental conditions the wells have no significant effect on the hydrophobicity of the membranes.

The high hydrophobicity, poor wettability, and low surface energy of fluorinated polymers can constitute a limitation in some applications were, for example, electrodes or other coating need to be deposited on its surface, as is the case of sensors, actuators, and energy harvesting devices. [33] Pillars-

TABLE 1 Images of the Contact Angle Measurements as a Function of Time of P(VDF-CTFE) Microstructures with Arrays of Pillars Obtained by Drying the Samples at 25°C Without and With Plasma Treatment

Without Plasma Treatment		With Plasma Treatment			
After 5 min	Dimensions	Before	At 0 s	At 5 s	At 15 s

	100 micrometers	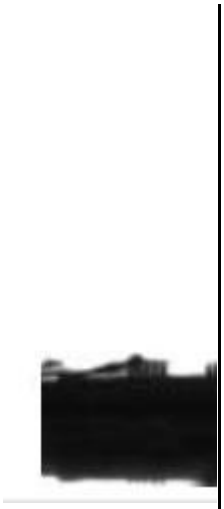	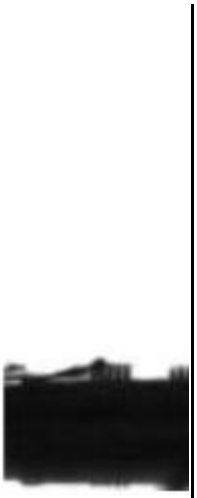		
	250 micrometers		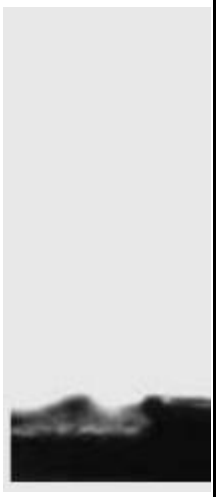		
	400 micrometers			7	7

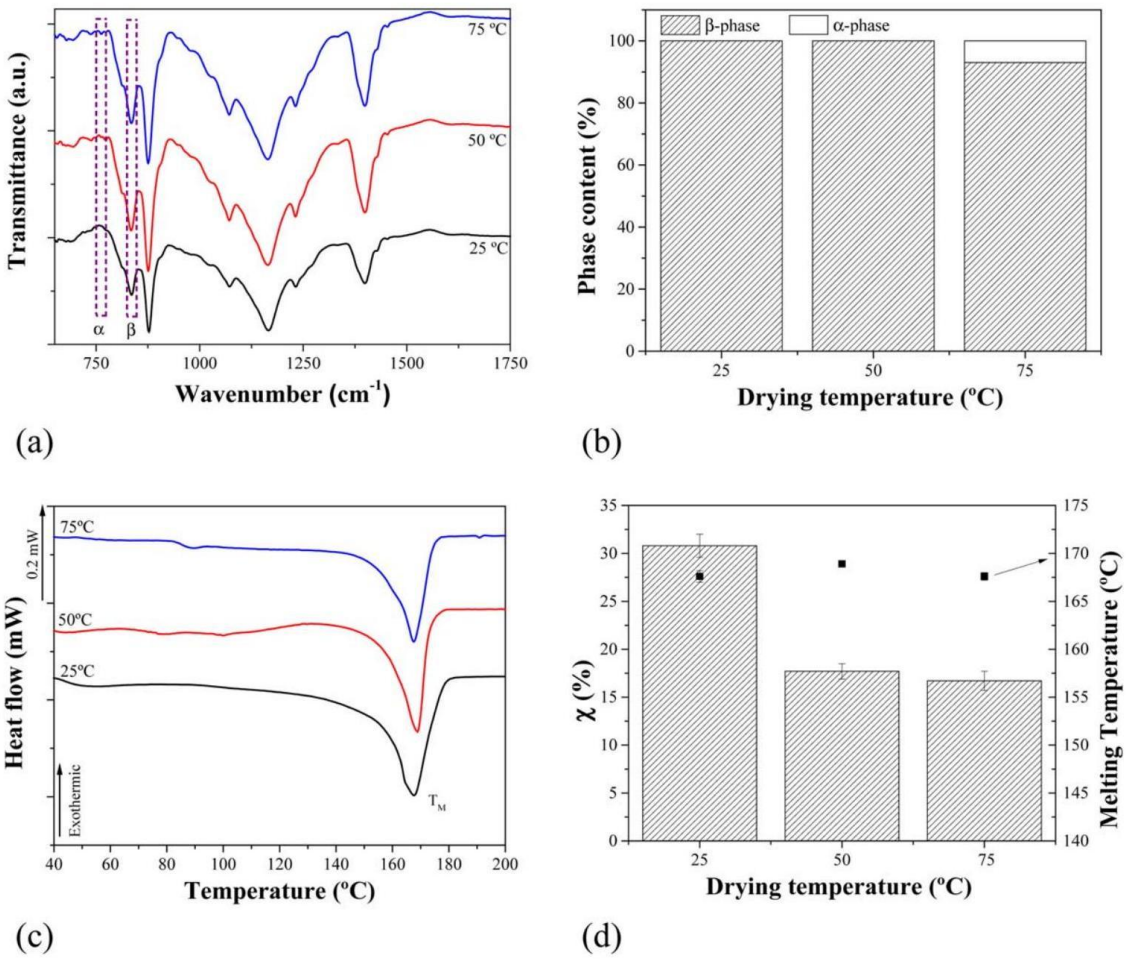

FIGURE 6 (a) FTIR-ATR spectra of the P(VDF-CTFE) samples dried at different temperatures; (b) respective α - and β-phases contents; (c) DSC scans of the P(VDF-CTFE) samples dried at different temperatures; (d) corresponding degree of crystallinity and melting temperature.

based P(VDF-CTFE) microstructures can work as sensors for the detection and quantification of biological entities, after the functionalization of the microstructures and/or the deposition of conductive electrodes. Thus, surface modification can be performed to tailor the copolymer wettability by changing the surface chemical composition by introducing specific functional groups on the surface either by chemical grafting or by using plasma treatment. [34,35] Plasma treatment using oxygen allows the incorporation of hydrophilic and oxygen functional groups and proved to be also effective on promoting cell growth on polymer surfaces. [36] Therefore, oxygen plasma treatments were performed with a plasma power of 100 W during 600 s on the superhydrophobic-based P(VDF-CTFE) microstructures, that is, constituted by pillars dried at 25 °C. [34] This plasma parameters were chosen accordingly to previous studies [34,37] to avoid heating and major structural surface modifications. Pictures of the contact angle measurements at different times are presented in Table 1.

It was proven that, under the used plasma treatment condition, the superhydrophobic surfaces of the pillars-based

microstructures can be modified to hydrophilic, being the results more significant for the 250 - and 400 − μm pillars where superhydrophilic surfaces were obtained. In the case of the 100 − μm pillars, the lower surface wettability modification is possibly related to the scale of the pillars arrays that prevents the spread of the water droplet. Furthermore, superhydrophilic surfaces were also obtained in the case of flat membranes and wells-based microstructures dried at 25 °C after plasma treatment. The surface modifications of the P(VDF-CTFE) samples after plasma treatment are attributed to the defluorination and oxidation reactions by the incorporation of oxygen onto the surfaces. In fact, oxygen plasma treatment should lead to cleavage of C-F and C-H hydrophobic groups followed by the formation of C = 0, OH and COOH hydrophilic groups on the surface of P(VDF-CTFE) copolymer, as already reported for PVDF. [34]

Crystalline Phase and Degree of Crystallinity

The identification of the crystalline phases of the processed samples is of major importance for application were piezoelectric properties are desired. [5,38] Fourier transformed

TABLE 2 Processing Conditions Used to Obtain the SU-8 Molds [42]

Conditions/SU-8 Thickness (μm)		100	250	400
Rotational speed (rpm)		3,200	2,100	1,200
Prebake time (min)	at 65 °C	20	35	45
	at 95 °C	40	70	150
UV exposure time (min)		6	9	12
Postbake time (min)	at 65 °C	5	10	20
	at 95°C	10	15	25
Development time (min)		8	20	30

infrared spectroscopy in attenuated total reflectance (FTIRATR) measurements were performed to identify the different crystalline phases presented in the flat and patterned P(VDFCTFE) microstructures [Fig. 6(a,b)]. Moreover, the presence of different morphologies and crystalline phases indicate a variation in the crystallization process of the P(VDF-CTFE) samples, as verified and discussed above, which in turn can lead to a variation in the degree of crystallinity. Therefore, DSC measurements were conducted to study possible variations of the melting temperature and degree of crystallinity. As for the crystalline phase description, the DSC results are presented accordingly to the drying temperature [Fig. 6(c, d)].

PVDF and its copolymers, as it is the case of P(VDF-CTFE), show strong absorption bands at 763 and 839 cm^{-1}, ascribed to the α - and β-phases, respectively. The β-phase content

within a sample is calculated measuring the absorbance at these two specific bands, according to the following equation. [8]

$$\%(\beta\text{-phase}) = \frac{A_\beta}{\frac{K_\beta}{K_\alpha} \times A_\alpha + A_\beta} \times 100 \quad (1)$$

where A_α and A_β represent the absorbance of the α - and β-phases at 763 and 839 cm^{-1}, respectively and K_α and K_β are the absorption coefficients at the respective wavenumber ($K_\alpha = 6.1 \times 10^4$ cm^2 mol^{-1}, $K_\beta = 7.7 \times 10^4$ cm^2 mol^{-1}).

The samples dried at the same temperature feature identical α - and β-phases content, independently of their flat or patterned microstructures, whereby the Figure 6(a,b) illustrates the FTIR-ATR spectra and the α - and β-phases content of the sample accordingly to the drying temperature, respectively.

The results demonstrated that, at drying temperatures of 25 and 50 °C, the P(VDF-CTFE) samples crystallize exclusively in the electroactive β-phase, whereas the samples dried at 75 °C show 7% of α-phase. At higher drying temperatures, it is expected that the α-phase content will increase inversely proportional to the amount of β-phase. [21,39] This result is explained due to the modified crystallization kinetics, an increase of the solvent evaporation rate and, therefore, of the crystallization rate of the copolymer favoring the formation of the α-phase of the copolymer. [21]

Regarding the DSC curves, the following equation was used to calculate the degree of crystallinity (χ),

$$\chi(\%) = \frac{\Delta H_\mathrm{m}}{a\Delta H_\alpha + b\Delta H_\beta} \times 100 \quad (2)$$

where ΔH_m is the melting enthalpy of the copolymer, a and b are the amount of α - and β-phases within the microstructures and ΔH_α and ΔH_β are the melting enthalpies for fully crystalline membranes of pure PVDF, exclusively in the α and β-phases, which is an appropriate approximation for the copolymers, with the values of 93.07 and 103.4 J g^{-1}, respectively. [40,41]

The DSC scans are characterized by a single endothermic peak, characteristic of the copolymer melting [Fig. 6(c)]. While the melting temperature of the P(VDF-CTFE) samples remains approximately constant with a mean value of 168°C regardless the processing conditions, the degree of crystallinity decreases from ~ 31 to 17% by increasing the drying temperature from 25 to 75 °C [Fig. 6(d)].

CONCLUSIONS

Patterned P(VDF-CTFE) microstructures in the electroactive polymer phase with tailored architecture, morphology and wettability were fabricated using simple, low cost and reproducible microfluidic strategies based on photolithography and replica molding techniques. Complex porous structures constitute by arrays of three-dimensional pillars or wells composed by large and nanoporous spherulites were obtained at a drying temperature of 25°C. At higher drying temperatures of 50 and 75 °C, the patterned P(VDF-

CTFE) microstructures present smoother surfaces and compact cross-sections. The fluorinate nature of the copolymer induces a hydrophobic behavior in all samples, being the threedimensional pillars-based microstructures superhydrophobic. Surface modification using plasma treatment with oxygen allowed reverse the reduced wettability of the samples making them hydrophilic and applicable in a wider range of applications. Further, the higher the drying temperatures between 25 and 75°C of the patterned P(VDF-CTFE) microstructures, lower is the electroactive β-phase content and the degree of crystallinity of the samples, ranging from 100 to 93 and 31 to 17%, respectively. Therefore, these complex

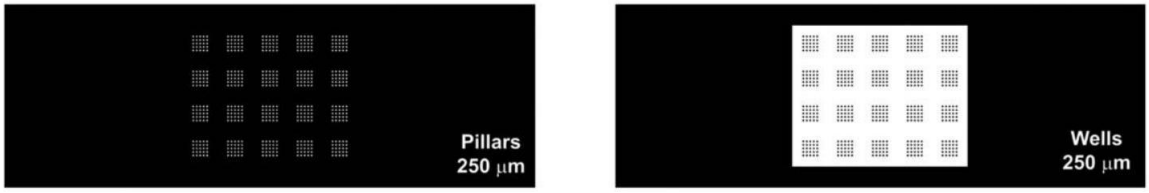

(a)
(b)

FIGURE 7 Examples of photomasks used in the UV exposure steps to create three SU-8 molds with arrays of (a) pillars of 100, 250 , and 400μ m and (b) wells with the same dimensions.

and novel platforms can represent innovative and advanced strategies in a wide range of biotechnological applications, including tissue engineering, drug delivery, microfluidic, and sensors and actuators devices.

EXPERIMENTAL

Materials

The materials used for the reported patterned microstructures fabrication were the SU-8 100 (epoxy-based negative photoresist) and Sylgard® 184 Silicone Elastomer (PDMS) purchased from Microchem and Dow Corning, respectively. Moreover, P(VDF-CTFE) (Solef 31508) and dimethylformamide (DMF, 99.5%) were supplied by Solvay and Merck, respectively. Isopropyl alcohol was obtained from Sigma Aldrich. Ultrapure water was prepared in our laboratory. All chemicals and solvents were used as received.

Fabrication of SU- 8 Molds

As referred previously, the first step consists in the fabrication of SU-8 molds [Fig. 1(a)], which was carried out through a low cost photolithography process. [42] Six microstructures with two different configurations (arrays of pillars or wells) and three different dimensions (diameter/height and diameter/depth of the pillars and wells, respectively, of ~ 100,250, and 400μ m, separated by the same distance) were fabricated using glass slide as substrate (26×76 mm). Details on the different processing steps and the corresponding parameters used to obtain the SU- 8 molds can be found in ref. 42. The SU-8 processing

conditions are presented in Table 2 and images of the photomasks used in the UV exposure step, which represent the design of the microstructures, are illustrated in Figure 7.

After the development step in which the SU-8 not exposed to UV is removed, the samples were properly cleaned with isopropyl alcohol, dried gently with compressed air, and the final SU- 8 molds were obtained.

Fabrication of PDMS Molds

Prior to the preparation of the PDMS solution composed of 10/1% wt of base/curing agent, the SU- 8 molds were surrounded by aluminum adhesive tape to form the walls to retain the PDMS solution [Fig. 1(b)]. After the proper mixture of the two compounds and removal of air bubbles using a home-made vacuum system, approximately 2 g of PDMS solution was deposited on each SU-8 molds and left to cure at 80°C during 2 h using a hot plate (Präzitherm PZ23-2).

Fabrication of Patterned P(VDF-CTFE) Microstructures

A solution of P(VDF-CTFE) was prepared using DMF as solvent in a copolymer volume fraction of 9% [39] The copolymer was dissolved in DMF at a temperature of 50°C under magnetic stirring until a transparent and homogeneous solution was obtained. After cooling to room temperature, the solution was transferred to the PDMS molds [Fig. 1(c)]. When air bubbles were present, a needle was used to remove them. Then, the PDMS molds fully filled with the copolymer solution were placed in an oven (UP Selecta 200208) at a specific temperature (25,50 , or 75 °C) during 1 week to guarantee the complete evaporation of the solvent and crystallization of the copolymer. [7] Finally, the patterned P(VDF-CTFE) microstructures were removed from the PDMS molds and characterized [Fig. 1(d)].

Some P(VDF-CTFE) microstructures were submitted to a plasma treatment to study the possibility of modifying the hydrophobicity of the microstructures. Plasma surface treatments were performed using a plasma chamber (PlasmaElectronic Diener) equipped with a 40 – kHz radio frequency plasma generator. Oxygen gas was used with a plasma power of 100 W applied for 600 s .

Characterization of the Patterned P(VDF-CTFE)

Microstructures

A scanning electron microscope (SEM) Quanta 650 FEG from FEI was used to obtain the surface and transversal morphologies of the patterned P(VDF-CTFE) microstructures. A DataPhysics OCA20 and ultrapure water (drop volume of 3μ L and rate of 0.5μ L s^{-1}) were used to determine the contact angles at the surface of the microstructures. Six

measurements were performed in each sample and the values presented as the average. The crystalline phases of the copolymer were evaluated after the infrared spectra obtained by FTIR-ATR mode using a Vertex 70 from Bruker with 16 scans in the range between 650 and 4000 cm^{-1} and resolution of 4 cm^{-1}. Differential scanning calorimetry (DSC) was performed with a DSC822e from Mettler Toledo. Pieces of approximately 4 mg were cut and placed into 40μ L aluminum pans. The samples were heated between 30 and 200 °C at a scanning rate of 10 °Cmin^{-1}.

ACKNOWLEDGMENTS

The authors thank the FCT - Fundação para a Ciência e Tecnologia - for financial support under project PTDC/EEI-SII/5582/

2014 and project UID/EEA/04436/2013 by FEDER funds through the COMPETE 2020-Programa Operacional Competitividade e Internacionalização (POCI) with the reference project POCI-01-0145-FEDER-006941. VFC, VCP, and PJS thank the FCT for the SFRH/BPD/98109/2013, SFRH/BD/81526/2011 and SFRH/BD/81562/2011 grants, respectively. Financial support from the Basque Government Industry Department under the ELKARTEK Program is also acknowledged. SLM thanks the Diputación Foral de Bizkaia for financial support under the Bizkaia Talent program; European Union's Seventh Framework Programme; Marie Curie Actions-People; Grant agreement no. 267230.

REFERENCES AND NOTES

1 J. Nunes-Pereira, S. Ribeiro, C. Ribeiro, C. J. Gombek, F. M. Gama, A. C. Gomes, D. A. Patterson, S. Lanceros-Mendez, Polym. Test. 2015, 44, 234-241.
2 M. Arruebo, WIREs Nanomed. Nanobiotechnol. 2012, 4, 1630.

3 C. M. Costa, A. California, V. F. Cardoso, V. Sencadas, L. C. Rodrigues, M. M. Silva, S. Lanceros-Méndez, Ferroelectrics 2012, 430, 103-107.
4 W. G. Kim, S. Nair, Chem. Eng. Sci. 2013, 104, 908-924.
5 V. F. Cardoso, S. O. Catarino, S. Lanceros-Mendez, G. Minas, In: ENBENG. 2011, IEEE; Lisbo, 2011.
6 A. Kumar, A. Srivastava, I. Y. Galaev, B. Mattiasson, Prog. Polym. Sci. 2007, 32, 1205-1237.
7 V. F. Cardoso, C. M. Costa, G. Minas, S. Lanceros-Mendez, Smart Mater. Struct. 2012, 21, 085020.
8 P. Martins, A. C. Lopes, S. Lanceros-Mendez, Prog. Polym. Sci. 2014, 39, 683-706.
9 V. Sencadas, R. Gregorio Filho, S. Lanceros-Mendez, J. NonCryst. Solids 2006, 352, 2226-2229.
10 J. Nunes-Pereira, V. Sencadas, V. Correia, V. F. Cardoso, W. Han, J. G. Rocha, S. Lanceros-Méndez, Compos. Part B 2015, 72, 130-136.
11 D. M. Correia, R. Gonçalves, C. Ribeiro, V. Sencadas, G. Botelho, J. L. G. Ribelles, S. Lanceros-Méndez, RSC Adv. 2014, 4, 33013-33021.
12 Z. Cui, E. Drioli, Y. M. Lee, Prog. Polym. Sci. 2014, 39, 164-198.
13 R. X. Han, J. Z. Jin, P. Khanchaitit, J. K. Wang, Q. Wang, Polymer 2012, 53, 1277-1281.
14 R. E. Sousa, J. C. C. Ferreira, C. M. Costa, A. V. Machado, M. M. Silva, S. Lanceros-Mendez, J. Polym. Sci. Part B Polym. Phys. 2015, 53, 761-773.
15 J. H. Koh, Y. W. Kim, J. T. Park, B. R. Min, J. H. Kim, Polym. Adv. Technol. 2008, 19,

1643-1648.
16 J. Tan, W. M. Saltzman, Biomaterials 2004, 25, 3593-3601.
17 B. Cetin, M. B. Ozer, M. E. Solmaz, Biochem. Eng. J. 2014, 92, 92-63.

18 V. F. Cardoso, S. O. Catarino, J. S. Nunes, L. Rebouta, J. G. Rocha, S. Lanceros-Méndez, G. Minas, IEEE Trans. Biomed. Eng. 2010, 57, 1184-1190.
19 D. C. Duffy, J. C. McDonald, O. J. A. Schueller, G. M. Whitesides, Anal. Chem. 1998, 70, 4974-4984.
20 J. C. McDonald, D. C. Duffy, J. R. Anderson, D. T. Chiu, H. K. Wu, O. J. A. Schueller, G. M. Whitesides, Electrophoresis 2000, 21, 27-40.
21 V. F. Cardoso, G. Minas, C. M. Costa, C. J. Tavares, S. Lanceros-Mendez, Smart Mater. Struct. 2011, 20, 087002.
22 X. Zhang, F. Shi, J. Niu, Y. G. Jiang, Z. Q. Wang, J. Mater. Chem. 2008, 18, 621-633.
23 E. Gogolides, K. Ellinas, A. Tserepi, Microelectr. Eng. 2015, 132, 135-155.
24 L. Melita, F. Gumrah, M. Amareanu, Membr. Water Treat. 2014, 5, 147-170.
25 E. Ostuni, C. S. Chen, D. E. Ingber, G. M. Whitesides, Langmuir 2001, 17, 2828-2834.
26 N. A. Ahmad, C. P. Leo, A. L. Ahmad, W. K. W. Ramli, Sep. Purif. Rev. 2015, 44, 109-134.
27 J. T. Simpson, S. R. Hunter, T. Aytug, Rep. Prog. Phys. 2015, 78, 086501.
28 K. Koch, W. Barthlott, Philos. Trans. R. Soc. A Math. Phys. Eng. Sci. 2009, 367, 1487-1509.
29 S. H. Kim, J. Adhesion Sci. Technol. 2008, 22, 235-250.
30 R. N. Wenzel, Ind. Eng. Chem. 1936, 28, 988-994.
31 M. Nosonovsky, B. Bhushan, Curr. Opin. Colloid Interface Sci. 2009, 14, 270-280.
32 P. Roach, N. J. Shirtcliffe, M. I. Newton, Soft Matter 2008, 4, 224-240.
33 A. Kaynak, T. Mehmood, X. J. Dai, K. Magniez, A. Kouzani, Materials 2013, 6, 3482-3493.
34 D. M. Correia, C. Ribeiro, V. Sencadas, B. Botelho, S. A. C. Carabineiro, J. L. Gomes Ribelles, S. Lanceros-Méndez, Prog. Org. Coat. 2015, 85, 151-158.
35 S. d. Valence, J. C. Tille, C. Chaabane, R. Gurny, M. L. Bochaton-Piallat, B. H. Walpoth, M. Möller, Eur. J. Pharm. Biopharm. 2013, 85, 78-86.
36 D. Mangindaan, I. Yared, H. Kurniawan, J. R. Sheu, M. J. Wang, J. Biomed. Mater. Res. Part A 2012, 100A, 3177-3188.
37 D. M. Correia, C. Ribeiro, G. Botelho, J. Borges, C. Lopes, F. Vaz, S. A. C. Carabineiro, A. V. Machado, S. Lanceros-Méndez, Appl. Surf. Sci. 2016, 371, 74-82.
38 C. Ribeiro, D. M. Correia, S. Ribeiro, V. Sencadas, G. Botelho, S. Lanceros-Méndez, Eng. Life Sci. 2015, 15, 351-356.
39 V. F. Cardoso, G. Botelho, S. Lanceros-Mendez, Mater. Des. 2015, 88, 390-397.
40 A. J. Lovinger, Developments in crystalline polymers. Springer Netherlands, London; 1982.
41 S. Lanceros-Mendez, J. F. Mano, A. M. Costa, V. H. Schmidt, J. Macromol. Sci. Phys. 2001, B40, 517-527.

42 V. C. Pinto, P. J. Sousa, V. F. Cardoso, G. Minas, Micromachines 2014, 5, 738-755.